Towards a computationally efficient free-surface groundwater flow boundary condition for large-scale hydrological modelling

M. Rahman[1], R. Rosolem[1,2], S. J. Kollet[3,4], and T. Wagener[1,2]

[1]Department of Civil Engineering, University of Bristol, UK
[2]Cabot Institute, University of Bristol, UK
[3]IBG-3, Research Centre Jülich, Germany
[4]Center for High-Performance Scientific Computing in Terrestrial Systems, Geoverbund ABC/J, Germany

Abstract

Shallow groundwater is a critical component of the terrestrial water cycle. It sustains baseflow in rivers, supplies root zones with soil moisture during dry periods, and directly influences the land-atmosphere exchange processes. Nonetheless, the integration of groundwater into large-scale hydrological models remains challenging. The most detailed way of representing groundwater dynamics is to incorporate three-dimensional, variably saturated flow processes in the subsurface representation of hydrological models. However, such detailed modelling is still a challenge for global hydrological applications, mainly due to its high computational demand. In this study, a free-surface boundary condition called the Groundwater Flow Boundary (GFB) is developed to represent groundwater dynamics in a more computationally-efficient manner than the full three-dimensional models do. We evaluate GFB using two synthetic test cases, namely an infiltration experiment and a tilted-v catchment, which focus on groundwater recharge and discharge processes, respectively. The simulation results from GFB are compared with a three-dimensional groundwater flow model and with an over-simplified approach using a free-drainage lower boundary condition to assess the impact of our assumptions on model results. We demonstrate that GFB is

computationally more efficient compared to the three-dimensional model with limited loss in model performance when simulating infiltration and runoff dynamics.

1. Introduction

The dynamics of shallow groundwater table affect the variability of soil moisture and evapotranspiration at the land surface [*Chen and Hu*, 2004; *Kollet and Maxwell*, 2008; *Lam et al.*, 2011; *Soylu et al.*, 2011]. Spatial variability of groundwater table depth (WTD) creates lateral groundwater flow, which sustains baseflow in rivers [e.g., *Miller et al.*, 2016]. Due to its importance, recent studies have strongly suggested that groundwater dynamics should not be ignored in large-scale hydrological modelling [*Clark et al.*, 2015].

Numerical modelling has long been a key approach to study the hydrological cycle given that observations only provide an incomplete picture [*Fan et al.*, 2013]. Contemporary hydrological models that focus on the terrestrial component of the water cycle can broadly be classified into three groups: catchment-scale hydrological models, global hydrological models, and land surface models [*Archfield et al.*, 2015]. At the catchment-scale, models that integrate both surface and groundwater fluxes in a spatially explicit manner have been utilized for a while [e.g., *Abbott et al.*, 1986; *Qu and Duffy*, 2007; *Smerdon et al.*, 2007; *Kollet and Maxwell*, 2008; *Shen and Phanikumar*, 2010; *Rahman et al.*, 2014]. These models can represent heterogeneity in the subsurface and simulate groundwater flow at high spatial and temporal resolutions. Their application has largely focused on understanding the detailed interactions of hydrologic processes over smaller domains (i.e., from catchments to river basins).

In contrast, global hydrological models operate (so far mainly) at relatively coarse spatial resolutions (order of 10 to 100 km) and often focus on streamflow simulations at continental to global scales [*Wood et al.*, 1997; *Arnell*, 1999; *Döll et al.*, 2003]. Classically, these models

generally considered a simplified representation of subsurface hydrology, either neglecting or strongly over-simplifying groundwater dynamics. In recent years, some global hydrological models have started to consider groundwater dynamics more explicitly [e.g., *de Graaf et al.*, 2015; *Sutanudjaja et al.*, 2018]. It has also been advocated that global models should capture the effects of heterogeneity in topography, soils, and vegetation on hydrological cycle better by operating at a higher spatial resolution (1 km) [*Wood et al.*, 2011; *Archfield et al.*, 2015; *Bierkens et al.*, 2015].

A comprehensive method of considering groundwater dynamics is to incorporate an integrated hydrological model into the global models. In recent years, it has been demonstrated that fully integrated hydrological models can be applied at a continental scale [*Keune et al.*, 2016; *Maxwell and Condon*, 2016]. However, due to its numerical complexity, such a modelling practice generally demands substantial computational resources, which limits our ability for more detailed analyses of uncertainties and consequently the impacts of underlying assumptions [*Beven and Cloke*, 2012; *Kelleher et al.*, 2017].

Several previous studies have proposed simplified parameterizations for groundwater dynamics to overcome the issue of computational burden while modelling the integrated surface-groundwater system at large (e.g., continental to global) scales. For instance, the land surface models were originally developed to simulate the exchange of water and energy between the land surface and atmosphere [*Pitman*, 2003]. Due to the importance of shallow groundwater dynamics on land surface processes, the land surface modelling community has proposed simplified parametrizations to simulate groundwater dynamics over large domains [*Yeh and Eltahir*, 2005a; *Niu et al.*, 2011; *Zeng et al.*, 2016; *Oleson et al.*, 2013]. These simplified methods consider either probability distributions of soil, vegetation, and topography across the model domain to incorporate the subgrid-scale variability of WTD

74 [e.g., *Yeh and Eltahir*, 2005b], or use an implicit representation of groundwater flow [e.g.,
75 *Famiglietti and Wood*, 1994; *Koster et al.*, 2000]. Nevertheless, to our knowledge, none of
76 these approaches has been tested against the results from a fully integrated three-dimensional
77 hydrological model using synthetic studies to evaluate the impact of assumptions inherent in
78 these different parameterizations. We believe this is an important and currently missing step
79 in model development, which would allow modellers to better identify advantages and
80 quantify limitations in the theoretical development of any approach prior to its
81 implementation in complex modelling frameworks [*Clark et al.*, 2015].

82 In this study, we introduce a new explicit and computationally-efficient approach for
83 representing groundwater flow processes, namely the Groundwater Flow Boundary (GFB).
84 Because of its computational efficiency, the GFB approach can potentially be applied to
85 simulate groundwater dynamics over large domains in global hydrological and land surface
86 modelling applications at high spatial and temporal resolutions. We present simulation
87 examples in comparison with the three-dimensional hydrological model ParFlow [*Ashby and*
88 *Falgout*, 1996; *Kollet and Maxwell*, 2006; *Maxwell*, 2013] to evaluate the proposed GFB
89 approach, including the impact of our assumptions.

90 **2. Theory of the Groundwater Flow Boundary (GFB) condition**

91 A detailed, physics-based subsurface representation generally solves Richards' equation
92 [*Richards*, 1931] on a three-dimensional grid (Figure 1a), where the mathematical problem is
93 closed via appropriate initial and boundary conditions. In contrast, Figure 1b illustrates the
94 free-drainage (FD) lower boundary condition approach below one-dimensional isolated
95 shallow soil columns neglecting groundwater, which has been adopted by many large-scale
96 models and later modified using simple groundwater storage and water table
97 parameterizations [*Bierkens*, 2015]. Figure 1c shows a schematic of the proposed modelling

framework in this study. In this approach, the vertical model domain is divided into a shallow soil column (discretized in several model grids) and a deep aquifer. In the shallow soil column, Richards' equation simulates the variably saturated flow of water in three spatial dimensions.

$$S_s S_w \frac{\partial \psi_s}{\partial t} + \varphi \frac{\partial S_w(\psi_s)}{\partial t} = \nabla . \mathbf{q} + q_s \quad (1)$$

$$\mathbf{q} = -K_s K_r \nabla(\psi_s - z)$$

where S_s is specific storage coefficient [L^{-1}], S_w is relative saturation [-], φ is porosity [-], ψ_s is subsurface pressure head [L], t is time [T], $\mathbf{q}$ is water flux [LT^{-1}], q_s is the source/sink term [LT^{-1}] (e.g., infiltration from precipitation or evaporation), K_s is saturated hydraulic conductivity [LT^{-1}], K_r is relative permeability [-], and z is the depth below surface [L]. In this equation, the negative z axis points downward starting at the land surface. The van Genuchten relationships [*van Genuchten*, 1980] are used to describe the relative saturation and permeability functions in Equation 1. The Neumann type boundary condition for Richards' equation can be written as

$$K_s K_r \nabla(\psi_s - z) = q_b \quad (2)$$

where q_b is the flux at the boundary [LT^{-1}].

In two spatial dimensions, the equation of transient groundwater flow in an unconfined aquifer can be written as [*Pinder and Bredehoeft*, 1968; *Prickett and Lonnquist*, 1971; *Meenal and Eldho*, 2011]

$$S_y \frac{\partial h}{\partial t} = \nabla(\boldsymbol{T_r} \nabla h) + q_r \quad (3)$$

$$h = {}^{\Delta z_a}/_{2} + \psi_a \quad (4)$$

where S_y is specific yield [-], h is the depth integrated hydraulic head in the aquifer [L], $\mathbf{T_r}$ is the transmissivity of the aquifer [L^2T^{-1}], q_r is recharge/discharge rate [LT^{-1}], Δz_a is aquifer thickness [L], and ψ_a is the pressure head in aquifer [L]. Note that $\mathbf{T_r}$ is calculated by integrating K_s over h. This approach assumes that the variation of the saturated depth (Δh) is negligible compared to its absolute value (i.e., $\Delta h << h$).

Assuming pressure and flux continuity at the interface between the aquifer and the overlying soil layer (Figure 1c)

$$\psi_s = \psi_a = \psi \tag{5}$$

$$q_b = q_r \tag{6}$$

Note that such assumption of pressure and flux continuity was proposed by *Kollet and Maxwell* [2006] to integrate subsurface and surface water flow. Equation 3 can be solved for q_r as follows

$$q_r = S_y \frac{\partial \mathrm{h}}{\partial t} - \nabla(\boldsymbol{T_r} \nabla h) \tag{7}$$

Substituting q_r in equation (2) for q_b at the interface results in

$$-K_s K_r \nabla(\psi - z) = S_y \frac{\partial \mathrm{h}}{\partial t} - \nabla(\boldsymbol{T_r} \nabla h) \tag{8}$$

Thus, the groundwater flow equation is introduced as the lower boundary condition of Richards' equation for the soil columns.

In the proposed approach, groundwater dynamics are simulated (Equation 3) in two spatial dimensions using a single model layer (Figure 1c), which is computationally more efficient than a full 3D model resolving also vertical flow components in the aquifer. In the theoretical development of the GFB, we apply two major assumptions: (1) the negligible variability of

saturated depth compared to its absolute value (i.e., $\Delta h << h$); and, (2) the linear interpolation of the pressure between the aquifer and overlying soil layer.

3. Methods

In this study, we use the three-dimensional hydrological model ParFlow. We implement GFB in ParFlow, which allows us to compare the proposed approach with a detailed 3D model of groundwater flow. The ParFlow model along with the GFB implementation and the setup of the numerical experiments are described below.

3.1. The physics-based hydrological model ParFlow

ParFlow solves Richards' equation in three spatial dimensions considering a cell-centred finite-difference/finite control volume approximation in space and an implicit backward Euler scheme in time. The subsurface-surface flow coupling is achieved by applying a free-surface overland flow boundary condition at the land surface [*Kollet and Maxwell*, 2006]. In this approach, the kinematic wave equation is solved at the interface between the land surface and subsurface considering pressure and flux continuity. Honouring the topographic slopes in an approximate fashion, a terrain following grid is implemented in ParFlow [*Maxwell*, 2013].

We consider three configurations of ParFlow to evaluate our proposed free-surface boundary condition that represents groundwater dynamics in this study (i.e., the GFB). The standard formulation (FULL hereafter) includes variably saturated groundwater flow from the bottom of the aquifer to the land surface in three spatial dimensions. The GFB configuration incorporates our proposed groundwater flow boundary condition (Section 2) in ParFlow approximating the aquifer in two spatial dimensions. In contrast, the FD configuration mimics the classical description of water flow through soil still available in many LSMs by implementing a free drainage boundary condition in ParFlow assuming water flow through the soil columns only along the vertical direction.

3.2. Setup of the numerical experiments

We evaluate our proposed modelling approach using two synthetic test cases, namely the infiltration and the tilted-v catchment experiments (similar to *Kollet et al.*, 2017). The infiltration experiment compares the variably saturated flow through subsurface after a precipitation event to assess the capability of the different model configurations (i.e., FULL, GFB, and FD) to simulate recharge. The tilted-v catchment experiment compares the discharge simulated by the three model configurations. The setup of the two experiments is described below.

3.2.1. Infiltration experiment

Figure 2a shows the model setup of the infiltration experiment. A model domain of 2,500 m^2 is discretized using a uniform lateral grid resolution ($\Delta x = \Delta y$) of 10 m, yielding 5 grid cells in both x and y dimensions in all three (i.e., FULL, GFB, and FD) model configurations. In the FULL configuration, a total subsurface depth of 100 m (motivated by the global pattern of WTD presented in *Fan et al.* [2013]) is divided into 2,000 layers considering a uniform vertical resolution of Δz = 5 cm. The lower boundary condition is assumed to be no-flow. The FD configuration considers only 10 m deep soil columns (similar to soil domains typically observed in land surface models) that are divided into 200 vertical layers approximating a uniform Δz = 5 cm. As mentioned in the previous section, a free-drainage boundary condition is applied at the bottom of the soil columns in FD. The GFB configuration also considers shallow soil columns extending 10 m downward starting at the land surface. The soil columns in GFB are divided into 200 vertical layers assuming a uniform Δz = 5 cm. Unlike the FD setup, a 90-m deep aquifer is included underneath the shallow soil columns in GFB. The shallow soil columns and the aquifer are integrated using the free-surface boundary condition at the interface as discussed in Section 2.

188 The simulation period considered in the infiltration experiment is 5 days, with a constant time
189 step of Δt = 15 min. A spatially uniform rainfall rate of 5 mmh^{-1} is applied over the model
190 domain for the first 10 hrs of the simulation period. The infiltration experiment is performed
191 for 12 soil textural classes (Table 1) [e.g., *Rawls et al.*, 1982; *Saxton and Rawls*, 2006;
192 *Ghanbarian-Alavijeh et al.*, 2010] and the results of the three model configurations (FULL,
193 GFB, FD) are compared. All soil types are prescribed in a spatially uniform manner.

194 3.2.2. Tilted-v catchment

195 The experimental setup of the tilted-v catchment is illustrated in Figure 2b. The model
196 domain considered in this experiment is 2.1 x 1.0 km that is slanted in the *x* and y-directions.
197 A 100 m wide channel is located in the centre of this slanted model domain with the outlet
198 located at *y*=0. The tilted-v catchment is discretized using 21 and 10 grid cells in *x* and *y*-
199 direction, respectively ($\Delta x = \Delta y$ = 100 m). The total subsurface depth is 100 m in FULL,
200 which is divided into 200 equal vertical grids considering Δz = 50 cm. In this configuration, a
201 no-flow boundary condition is prescribed at the bottom of the model domain (i.e., 100 m
202 below surface). The GFB configuration, in contrast, considers a 90-m thick aquifer that is
203 overlain by soil columns extending 10 m below surface. A uniform vertical grid spacing of
204 Δz = 50 cm is used to divide the 10-m soil columns of GFB into 20 model layers. Identical to
205 the infiltration experiment, these soil columns are coupled to the aquifer using our proposed
206 free-surface boundary condition (i.e., the GFB) at the interface. A simulation period of 20 h is
207 considered for this experiment with a constant Δt = 15 min. Groundwater table (WT) is
208 initially located at the land surface and no rainfall is applied in this experiment. Notice that
209 the FD experiment does not solve for lateral flow, hence there is no expected contribution to
210 discharge in the tilted-v catchment experiment. For this reason, the FD configuration is
211 excluded form this experiment. As with the infiltration experiment, all soil types are
212 uniformly prescribed in the tilted-v experiment.

213 ## 4. Results and discussion

214 ### 4.1. Infiltration experiment

215 The goal of this experiment is to assess how the wetting front from a specific rainfall event
216 develops and further interacts with a pre-defined water table within the domain for all three
217 model configurations. Figure 3 compares relative soil moisture (S_w) profiles (0-2.5 m below
218 land surface) from infiltration experiment simulated by the three model configurations, i.e.,
219 FULL, GFB, and FD for a silty soil. Note that only the S_w profiles from the central cell of the
220 model domain (Figure 2) are presented here.

221 In all three configurations, the relatively shallow soil layers are initially dry because the
222 groundwater table is located at 1.5 m below the land surface. Infiltration starts immediately
223 with the onset of the precipitation in all three cases, which is observed by the increased
224 saturation level of the soil layers starting at the top of the profiles. After about 5 h, the
225 infiltration front reaches the groundwater table (WT) in FULL. The shallow S_w simulated by
226 this configuration gradually decreases as the infiltration front moves deeper once the
227 precipitation ceases.

228 The movement of the infiltration front in GFB generally agrees well with that of the FULL
229 configuration. Figure 3b shows that the rise and recession of the WT due to the precipitation
230 event is captured by GFB. Though, it appears that groundwater recharge simulated by GFB is
231 smaller compared to the FULL configuration. During the recession, the shallow soil layers
232 dry out faster in GFB. The S_w profile simulated by FD, on the other hand, dries out
233 considerably faster compared to both FULL and GFB. While the WT was initially located at
234 1.5 m below surface in all three configurations, it quickly moves deeper in FD due to the
235 persistent gravity drainage imposed by the lower boundary condition, which is intuitive.

Both GFB and FD show differences in simulated soil moisture compared to FULL (Figure 3). We quantify these differences in S_w profiles using Mean Difference (MD), which is calculated as

$$MD = \frac{1}{nt}\frac{1}{nd}\sum_{i=1}^{i=nt}\sum_{j=1}^{j=nd}\left(a_{i,j} - b_{i,j}\right) \quad (9)$$

where MD is the mean difference between the soil moisture profiles a and b, t is the time instance, and d denotes soil layer. Note that only the soil columns up to 10 m below surface from the three model configurations are considered in the calculation of MD. This analysis reveals that MD is 0.0081 for GFB, while the FD configuration shows an MD = 0.0909 (Figure 3). GFB, therefore, performs substantially better than FD in reproducing the S_w profile simulated by the FULL configuration for silty soil.

The numerical experiment described in Figure 3 gives us some initial insight into the performance of our newly proposed approach in comparison with the FULL and FD configurations, respectively. We further expand this experiment by evaluating the performance of GFB against FULL and FD for 12 soil textural classes (Table 1) following the same initialization procedure described for the silty soil simulations in Figure 3. Figure 4 shows the MD of S_w profiles simulated by GFB and FD compared to that of FULL for 12 soils. The best performance of GFB is observed for clay soil with an MD of 10^{-4}. The largest difference between the S_w profiles from the two configurations is observed for sand, which is indicated by the largest MD = 0.034. Such model behaviour is observed due to the linear interpolation of pressure between the aquifer and lowermost soil layer, which is a key assumption in the formulation of GFB. For a fine-textured soil (e.g., clay) the saturation-pressure head relationship is linear in the van Genuchten relationship [e.g., *Assouline et al.*, 1998]. However, a coarse-textured soil (e.g., sand) shows non-linear behaviour, which weakens our assumption of a linear pressure profile between the lowest soil layer and aquifer.

For the FD configuration, the MD also increases for relatively coarse-textured soils, which is consistent with GFB. However, differences are systematically larger for FD in comparison to the differences observed in GFB for all soil types. In general, FD substantially underestimates S_w compared to FULL (MD > 0) due to the prescribed free-drainage lower boundary condition. The best model performance is again observed for clay soil with an MD = 0.0124. In contrast, sand shows an MD = 0.4937, indicating differences between the S_w profiles simulated by FULL and FD. Therefore, Figure 4 indicates that GFB performs considerably better than FD in reproducing FULL simulated S_w for all soil classes.

The results discussed in Figures 3 and 4 focused on understanding the sensitivity of the dynamic differences in soil wetness from the three configurations for various soil classes. Another important aspect of our model development is to test how these configurations behave under different initial WTD conditions. Figure 5 shows the MD between the S_w profiles from the FULL and GFB configurations for 12 soil types (Table 1) considering a number of initial depths of WT. The result demonstrates that for an initial WTD > 20 m, the S_w profiles from FULL and GFB are identical for all soil types. For WTD ≤ 20m, the discrepancies between the two configurations increase from fine to coarse-textured soils due to the assumption of a linear pressure profile between the lowest soil layer and aquifer. The differences between the S_w profiles for clay at all initial WT are negligible. The loam soil shows higher MD compared to clay, which reaches its maximum (MD = 0.014) for an initial WT located at 10 m below land surface. For sand, the highest MD = 0.068 is observed when WT is initially located at 7 m below the land surface. Therefore, for fine-textured soils (e.g., clay), the S_w profiles from FULL and GFB generally agree well. However, in coarse-textured soils (e.g., sand), differences between the FULL and GFB configurations are relatively high for 0.25 m ≤ WTD ≤ 20 m.

It has been discussed earlier that the FULL and GFB configurations consider 2000 (up to 100 m below surface) and 200 (up to 10 m below surface) vertical model layers, respectively in the infiltration experiment. Because of this difference in vertical model layers, the total computing time required (t_{cpu}) by the two configurations to perform this experiment will vary. Figure 6 shows the t_{cpu} of FULL and GFB for different soil textures presented in Table 1 with initial WT located at 1.5 m below surface. This plot clearly shows that the t_{cpu} of GFB is considerably lower than that of FULL for all soil types. This is also substantiated by the mean t_{cpu} of 272 s and 42 s over all the soil types for the FULL and GFB configurations, respectively. In summary, Figure 6 demonstrates that the t_{cpu} of GFB is about 6 times lower than that of FULL, which indicates that the former is computationally much more efficient.

4.2. Tilted-v catchment

The previous section evaluated GFB considering a test case focusing on infiltration. In this section, we test the capability of the GFB approach to simulate discharge due to lateral groundwater flow in a tilted-v catchment. Figure 7 shows cumulative discharge at the outlet of the tilted-v catchment (Figure 2b) from FULL and GFB. Note that the soil hydraulic properties of loam soil (Table 1) is considered in these simulations. Along the *x*- and y- axis, topographic slopes (*SL*) of $SL_x = 0.005$ and $SL_y = 0.002$ (Figure 2b) are prescribed in this numerical experiment. The WT is located at the land surface initially (WTD = 0) in both configurations. Figure 7 shows that GFB marginally underestimates the discharge simulated by FULL. Despite this underestimation, good overall agreement between the discharge simulated by FULL and GFB is observed (i.e., low MD of 0.002 m^3s^{-1} between the discharge time series simulated by the two configurations).

The required CPU time (t_{cpu}) to simulate the tilted-v experiment by the FULL and GFB configurations are 35 s and 8 s, respectively. As discussed in section 3.2.2, the FULL

configuration considers 200 vertical model grid cells for the tilted-v catchment. In contrast, the GFB configuration consists 20 grid cells below surface, which is the reason of discrepancies between the t_{cpu} from the two configurations. This difference in t_{cpu} shows that GFB is computationally more efficient than FULL in simulating the tilted-v catchment, which is consistent with the results from the infiltration experiment.

Figure 8 shows the flow depth along the x-axis of the tilted-v catchment at y = 500 m (see Figure 2) at different simulation times. This figure shows low flow depth close to the lateral boundaries (i.e., x = 0 and x = 2100 m), which increases gradually towards the central channel. The maximum flow depth is observed at the channel of the catchment. At t = 1 h, GFB underestimates flow depth compared to the FULL configuration. This underestimation of flow depth is consistent with the lower discharge simulated by GFB observed in Figure 7. At t = 5 h and 10 h, the GFB performs well in reproducing the flow depth simulated by FULL. In contrast, slight overestimation of the flow depth by GFB is observed at t = 15 h. The spatial variability of the flow depth observed in Figure 8 occurs due the effect of topographic slopes that forces groundwater to converge at the central channel of the catchment. This figure demonstrates that the overall variability of flow depth along the topographic slopes simulated by FULL is reproduced well by the GFB configuration.

We now assess the impact of soil types on the differences between discharge simulated by FULL and GFB. Figure 9 compares the differences between FULL and GFB simulated cumulative discharge at the outlet of tilted-v catchment considering three different soil types, i.e., sand, loam, and clay (coarse, medium, and fine-textured, respectively). Note SL_x = 0.005 and an initial WTD = 0 is considered in this experiment, which is identical to that of Figure 8. The smallest difference between FULL and GFB is observed for clay soil in Figure 9. For sand, on the other hand, the largest difference between FULL and GFB simulated cumulative discharge is noted. The MD between FULL and GFB simulated discharge for clay, loam, and

sand are $9x10^{-7}$, 0.0018, and 0.0420 m^3s^{-1}, respectively. This analysis shows that the differences between runoff from the two configurations increase from fine to coarse-textured soils, which is consistent with the infiltration experiment.

As a final test, we investigate the sensitivity of runoff from GFB due to different topographic slopes along the x-axis (SL_x) of the tilted-v catchment considering the same initialization steps in Figure 8. Figure 10a plots the MD between runoff from the GFB and FULL configurations as a function of SL_x. In general, the runoff from GFB compares well with that of FULL for all SL_x, which is indicated by the low MD values (on the order of 10^{-3} to 10^{-2} m^3s^{-1}). Figure 10a demonstrates that differences between FULL and GFB simulated discharge generally increase from mild to steep SL_x. For $SL_x \leq 0.01$, GFB underestimates (MD > 0) runoff compared to FULL. For higher SL_x values, in contrast, overestimation (MD < 0) of runoff by GFB is observed.

Figure 10b presents the t_{cpu} from the FULL and GFB configurations to simulate tilted-v experiment as a function of topographic slope (SL_x). This figure depicts that the t_{cpu} required by GFB is very low compared to that of FULL. The t_{cpu} of FULL increases from mild to steep SL_x. The minimum (35 s) and maximum (794 s) t_{cpu} of FULL are observed for $SL_x = 0.005$ and 0.25, respectively. In contrast to FULL, the maximum t_{cpu} required by GFB is 8 s, which is observed for $SL_x = 0.25$. The mean t_{cpu} values over all slopes are 322 s and 7 s, respectively for FULL and GFB. H Therefore, our proposed approach is about 43 times faster than the FULL configuration.

In this study, we have presented an efficient approach of representing groundwater dynamics in large-scale numerical models by reducing the number of computational nodes in the vertical direction. It is important to note that previous studies have also proposed an "effective hillslope" concept that adopts a pseudo 2-D approach to reduce the computational

357 demand of simulating the lateral groundwater flow in hydrological models [*Troch et al.*,
358 2003; *Hazenberg et al.*, 2015]. This concept can be applied in conjunction with our proposed
359 GFB to further enhance the computational efficiency of the large scale hydrological models.

360 **5. Summary and conclusions**

361 We have proposed a novel free-surface Groundwater Flow Boundary (GFB) condition to
362 parameterize groundwater dynamics in land surface or large-scale hydrological models that
363 require representation of groundwater dynamics in an efficient manner. In our approach, the
364 groundwater flow in an unconfined aquifer acts as the lower boundary condition for the of
365 shallow soil columns assuming pressure and flux continuity at the soil-aquifer interface. The
366 two major assumptions in the GFB approach are: (1) the pressure profile can be linearly
367 interpolated from the aquifer to the first computation node at the bottom of the soil column;
368 and (2) the variability of saturated depth is negligible compared to its absolute value. Three
369 model configurations, (i.e., namely FULL, GFB, and FD) are compared to evaluate the
370 proposed approach and the impact of the assumptions using two synthetic experiments
371 focusing on groundwater recharge (infiltration experiment) and contribution from
372 groundwater to discharge (tilted-v experiment), respectively. The FULL configuration
373 represents a detailed three-dimensional physics-based hydrological model with deep soil
374 columns. In FD, a gravity drainage boundary condition is applied below shallow soil columns
375 mimicking the classical large-scale land surface modelling approach that neglects
376 groundwater dynamics. In contrast, the GFB configuration prescribes our proposed boundary
377 condition below shallow soil columns representing simplified groundwater dynamics
378 compared to FULL.

379 From the results of the infiltration experiment, it is evident that GFB performs considerably
380 better in simulating soil water movement compared to FD, which is consistent across all soil

textural classes. The best performance of the GFB configuration relative to FULL is observed across fine-textured soils (e.g., clay). For coarse-textured soils (e.g., sand), however, the differences between FULL and GFB increased as a result of the assumptions introduced in GFB. For the tilted-v experiment, runoff is generated solely due to the convergence of groundwater along the central channel (i.e., no rainfall is applied). At the outlet of the catchment, the cumulative discharge volumes from the FULL and GFB agree well. Our results also demonstrate that the GFB configuration can reproduce the spatial variability of the flow depth well when compared to FULL. The advantage of using GFB is highlighted in this synthetic case by a much lower computing time compared to the FULL configuration.

Our model evaluation suggests that GFB can potentially be used to represent groundwater dynamics in large-scale hydrological and land surface modelling applications, especially given its computational efficiency while resulting in relatively minimal loss of performance when compared to a more detailed and integrated hydrological model. It is, however, important to emphasize that our study focuses only on the evaluation of the proposed approach using two synthetic test cases, which consider, for instance, homogeneous soils, simplified topographic slopes, and uniform atmospheric forcing. The GFB approach certainly requires additional corroboration considering real-world and larger model domains studies, including heterogeneity in relief, soil information, and atmospheric forcing.

Acknowledgements

We gratefully acknowledge the support by the "A MUlti-scale Soil moisture Evapotranspiration Dynamics study" (AMUSED) [grant number NE/M003086/1] and the "Brazilian Experimental datasets for MUlti-Scale interactions in the critical zone under Extreme Drought" (BEMUSED) [grant number NE/R004897/1], both projects funded by Natural Environment Research Council (NERC). Partial support from the NERC "Managing the Risks, Impacts and Uncertainties of drought and water Scarcity" (MaRIUS) project [grant number NE/L010399/1] received by Thorsten Wagener is appreciated and gratefully acknowledged. We would also like to acknowledge the partial support by the Queens School Pump-Priming grant 2016 (University of Bristol). We also appreciate the comments and suggestions from the three anonymous reviewers and the editor, which all helped to improve the quality of this manuscript.

425 **References**

426 Abbott, M. B., J. C. Bathurst, J. A. Cunge, P. E. O'Connell, and J. Rasmussen (1986), An
427 introduction to the European Hydrological System — Systeme Hydrologique Europeen,
428 "SHE", 1: History and philosophy of a physically-based, distributed modelling system, J.
429 Hydrol., 87, 45-59, doi:10.1016/0022-1694(86)90114-9.

430 Archfield, S. A., M. Clark, B. Arheimer, L. E. Hay, H. McMillan, J. E. Kiang, J. Seibert, K.
431 Hakala, A. Bock, T. Wagener, W. H. Farmer, V. andréassian, S. Attinger, A. Viglione, R.
432 Knight, S. Markstrom, and T. Over (2015), Accelerating advance sin continental domain
433 hydrologic modeling, Water. Resour. Res., 51, 10078-10091, doi:10.1002/2015WR017498.

434 Arnell, N. W. (1999), A simple water balance model for the simulation of streamflow over a
435 large geographic domain, J. Hydrol., 217, 314-335.

436 Ashby, S. F., and R. D. Falgout (1996), A parallel multigrid preconditioned conjugate
437 gradient algorithm for groundwater flow simulations, Nucl. Sci. Eng., 124(1), 145– 159.

438 Assouline, S., D. Tessier, and A. Bruand (1998), A conceptual model of the water retention
439 curve, Water Resour. Res., 34(2), 223-231.

440 Beven, K. J. and H. L. Cloke (2012), Comment on: Hyperresolution global land surface
441 modeling: Meeting a grand challenge for monitoring Earth's terrestrial water by Eric F Wood
442 et al. Water Resources Research, 48 (1). W01801. ISSN 00431397 doi:
443 https://doi.org/10.1029/2011WR010982.

444 Bierkens, M. F. P. (2015), Global hydrology 2015: State, trends, and directions, Water
445 Resour. Res., 51, 4923-4947, doi:10.1002/2015WR017173.

446 Chen, X., and Q. Hu (2004), Groundwater influences on soil moisture and surface
447 evaporation, J. Hydrol., 297, 285-300.

448 Clark, M. P., Y. Fan, D. M. Lawrence, J. C. Adam, D. Bolster, D. J. Gochis, R. P. Hooper,
449 M. Kumar, L. R. Leung, D. S. Mackay, R. M. Maxwell, C. Shen, S. C. Swenson, and X. Zeng
450 (2015), Improving the representation of hydrologic processes in Earth System Models, Water
451 Resour. Res., 51, 5929– 5956, doi:10.1002/2015WR017096.

452 Döll, P., F. Kaspar, and B. Lehner (2003), A global hydrological model for deriving water
453 availability indicators: Model tuning and validation, J. Hydrol., 270(1–2), 105–134,
454 doi:10.1016/S0022-1694(02)00283-4.

455 Famiglietti, J. S., and E. F. Wood (1994), Multiscale modeling of spatially variable water and
456 energy balance processes, Water Resour. Res., 30(11), 3061-3078.

457 Fan, Y., H. Li, and G. Miguez-Macho (2013), Global pattern of groundwater table depth,
458 Science, 339(6122), 940-943, doi: 10/1126/science.1229881.

459 Hazenberg, P., Y. Fang, P. Broxton, D. Gochis, G.-Y. Niu, J. D. Pelletier, P. A. Troch, and X.
460 Zeng (2015), A hybrid-3D hillslope hydrological model for use in Earth system models,
461 Water Resour. Res., 51, 8218–8239, doi:10.1002/2014WR016842.

462 Kelleher, C., McGlynn, B. and Wagener, T. (2017), Characterizing and reducing equifinality
463 by constraining a distributed catchment model with regional signatures, local observations,
464 and process understanding. Hydrol. Earth Syst. Sci., 21, 3325–3352, doi.org/10.5194/hess-
465 21-3325-2017.

Keune, J., F. Gasper, K. Goergen, A. Hense, P. Shrestha, M. Sulis, and S. Kollet (2016), Studying the influence of groundwater representations on land surface-atmosphere feedbacks during the European heatwave in 2003, J. Geophys. Res. Atmos. 121, 13301-13325.

Kollet, S. J., and R. M. Maxwell (2006), Integrated surface-groundwater flow modeling: A free-surface overland flow boundary condition in a parallel groundwater flow model, Adv. Water Resour., 29(7), 945– 958.

Kollet, S. J., and R. M. Maxwell (2008), Capturing the influence of groundwater dynamics on land surface processes using an integrated, distributed watershed model, Water Resour. Res., 44, W02402, doi:10.1029/2007WR006004.

Kollet, S., M. Sulis, R. M. Maxwell, C. Paniconi, M. Putti, G. Bertoldi, E. T. Coon, E. Cordano, S. Endrizzi, E. Kikinzon, E. Mouche, C. Mügler, Y.-j. Park, J. C. Refsgaard, S. Stisen, and E. Sudicky (2017), The integrated hydrologic model intercomparison project, IH-MIP2: A second set of benchmark results to diagnose integrated hydrology and feedbacks, Water Resour. Res., 53, 867-890, doi:10.1002/2016WR019191.

Koster, R. D., M. J. Suarez, A. Ducharne, M. Stieglitz, and P. Kumar (2000), A catchment-based approach to modeling land surface processes in a general circulation model 1. Model structure, J. Geophys. Res., 105(D20), 24,809-24,822.

Lam, A., D. Karssenberg, B. J. J. M. van den Hurk, and M. F. P. Bierkens (2011), Spatial and temporal connections in groundwater contribution to evaporation, Hydrol. Earth Syst. Sci., 15, 2621–2630.

Maxwell, R. M. (2013), A terrain-following grid transform and preconditioner for parallel, large-scale integrated hydrologic modeling, Adv. Water Resour., 53, 109-117.

488 Maxwell, R. M. and L. E. Condon (2016), Connections between groundwater flow and
489 transpiration partitioning. Science, 353:6297, 377-380, doi:10.1126/science.aaf7891.

490 Meenal, M., and T. I. Eldho (2011), Simulation of groundwater flow in unconfined aquifer
491 using meshfree point collocation method, Eng. Anal. Bound. Elem., 35, 700-707,
492 doi:10.1016/j.enganabound.2010.12.003.

493 Miller, M. P., S. G. Buto, D. D. Susong, and C. A. Rumsey (2016), The importance of base
494 flow in sustaining surface water flow in the Upper Colorado River Basin, Water Resour. Res.,
495 52, 3547–3562, doi:10.1002/2015WR017963.Niu, G.-Y., Z.-L. Yang, K. E. Mitchell, F. Chen,
496 M. B. Ek, M. Barlage, A. Kumar, K. Manning, D. Niyogi, E. Rosero, M. Tewari, and Y. Xia
497 (2011), The community Noah land surface model with multiparameterization options (Noah-
498 MP): 1. Model description and evaluation with local-scale measurements, J. Geophys. Res.,
499 116, D12109, doi:10.1029/2010JD015139.

500 Oleson, K. W., et al. (2013), Technical description of version 4.5 of the Community Land
501 Model (CLM), National Center for Atmospheric Research, Boulder, Colo.

502 Pinder, G. F., and J. D. Bredehoeft (1968), Application of the digital computer for aquifer
503 evaluation, Water Resour. Res., 4, 1069-1093.

504 Pitman, A. J. (2003), The evolution of, and revolution in, land surface schemes designed for
505 climate models, Int. J. Climatol., 23, 479-510, DOI: 10.1002/joc.893.

506 Prickett, T. A., and C. G. Lonnquist (1971), Selected Digital Computer Techniques for
507 Groundwater Resource Evaluation. Illinois State Water Survey, Urbana, Bulletin 55, 3-5.

508 Qu, Y., and C. Duffy (2007), A semidiscrete finite volume formulation for multiprocess
509 watershed simulation, Water Resour. Res., 43, W08419, doi:10.1029/2006WR005752, 2007.

510 Rahman, M., M. Sulis, and S. J. Kollet (2014), The concept of dual-boundary forcing in land
511 surface-subsurface interactions of the terrestrial hydrologic and energy cycles, Water Resour.
512 Res., 50, 8531‐8548, doi:10.1002/2014WR015738.

513 Richards, L. A. (1931), Capillary conduction of liquids through porous mediums, Physics, 1,
514 318.

515 Shen, C., and M. S. Phanikumar (2010), A process-based, distributed hydrologic model based
516 on a large-scale method for surface–subsurface coupling, Adv. Watr Resour., 33, 1524-1541,
517 doi:10.1016/j.advwatres.2010.09.002.

518 Smerdon, B. D., C. A. Mendoza, and K. J. Devito (2007), Simulations of fully coupled lake-
519 groundwater exchange in a subhumid climate with an integrated hydrologic model, Water
520 Resour. Res., 43, W01416, doi:10.1029/2006WR005137.

521 Soylu, M. E., E. Istanbulluoglu, J. D. Lenters, and T.Wang (2011), Quantifying the impact of
522 groundwater depth on evapotranspiration in a semi-arid grassland region, Hydrol. Earth Syst.
523 Sci., 15, 787–806.

524 Sutanudjaja, E. H., R. van Beek, N. Wanders, Y. Wada, J. H. C. Bosmans, N. Drost, R. J. van
525 der Ent, I. E. M. de Graaf, J. M. Hoch, K. de Jong, D. Karssenberg, P. López López, S.
526 Peßenteiner, O. Schmitz, M. W. Straatsma, E. Vannametee, D. Wisser, and M. F. P. Bierkens
527 (2018), PCR-GLOBWB 2: a 5 arcmin global hydrological and water resources model,
528 Geosci. Model Dev., 11, 2429–2453, https://doi.org/10.5194/gmd-11-2429-2018.

529 Troch, P. A., C. Paniconi, and E. E. van Loon (2003), Hillslope-storage Boussinesq model for
530 subsurface flow and variable source areas along complex hillslopes: 1. Formulation and
531 characteristic response, Water Resour. Res., 39(11), 1316, doi:10.1029/2002WR001728.

Van Genuchten, M. Th. (1980), A closed-form equation for predicting the hydraulic conductivity of unsaturated soils, Soil Sci. Soc. Am. J., 44,892-898.

Wood, E. F., D. Lettenmaier, X. Liang, B. Nijssen, and S. W. Wetzel (1997), Hydrological modeling of continental-scale basins, Annu. Rev. Earth Planet. Sci., 25, 279-300.

Wood, E. F., J. K. Roundy, T. J. Troy, L. P. H. van Beek, M. F. P. Bierkens, E. Blyth, P. Döll, M. Ek, J. Famiglietti, D. Gochis, N. van de Giesen, P. Houser, P. R. Jaffé, S. Kollet, B. Lehner, D. P. Lettenmaier, C. Peters-Lidard, M. Sivapalan, J. Sheffield, A. Wade, and P. Whitehead (2011), Hyperresolution global land surface modeling: Meeting a grand challenge for monitoring Earth's terrestrial water, Water Resour. Res., 47, W05301, doi:10.1029/2010WR010090.

Yeh, P. J.-F, and E. A. B. Eltahir (2005a), Representation of water table dynamics in a land surface scheme. Part I: model development, J. Climate, 18, 1861-1880.

Yeh, P. J.-F, and E. A. B. Eltahir (2005b), Representation of water table dynamics in a land surface scheme. Part II: subgrid variability, J. Climate, 18, 1881-1901.

Zeng, Y., Z. Xie, Y. Yu, S. Liu, L. Wang, J. Zou, P. Qin, and B. Jia (2016), Effects of anthropogenic water regulation and groundwater lateral flow on land processes, J. Adv. Model. Earth Syst., 8, 1106–1131, doi:10.1002/2016MS000646.

Tables

Table 1. Hydraulic properties for various soil texture classes (sources: *Johnson et al.*, 1967; *Rawls et al.*, 1982; *Schaap and Leij*, 1998; *Saxton and Rawls*, 2006; *Ghanbarian-Alavijeh et al.*, 2010).

Index	Texture	K_s (ms^{-1})	φ (-)	S_y (%)
1	Clay	$1.7x10^{-7}$	0.459	2
2	Clay loam	$9.4x10^{-7}$	0.442	4
3	Silty clay	$1.1x10^{-6}$	0.481	1
4	Silty clay loam	$1.2x10^{-6}$	0.482	3
5	Sandy clay	$1.3x10^{-6}$	0.385	7
6	Loam	$1.4x10^{-6}$	0.399	11
7	Sandy clay loam	$1.5x10^{-6}$	0.384	10
8	Silt loam	$2.1x10^{-6}$	0.439	5
9	Sandy loam	$4.4x10^{-6}$	0.387	12
10	Silt	$5.1x10^{-6}$	0.489	8
11	Loamy sand	$1.2x10^{-5}$	0.390	22
12	Sand	$5.8x10^{-5}$	0.375	25

Figures

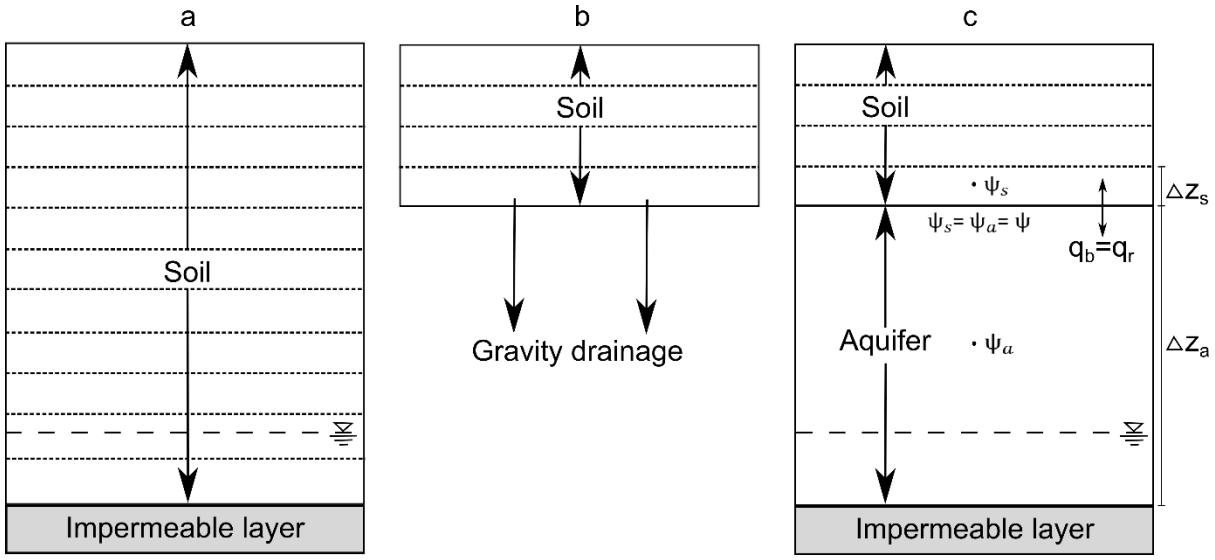

Figure 1. Schematic of the vertical extent of (a) a detailed hydrological model, (b) a large-scale model with typically applied free-drainage boundary condition, and (c) the proposed modelling approach of this study (referred as Groundwater Flow Boundary; GFB). While the dotted lines in the figure represent vertical grid discretization, the dashed lines show the location of the groundwater table depth. For clarity, the schematic depicts a column system.

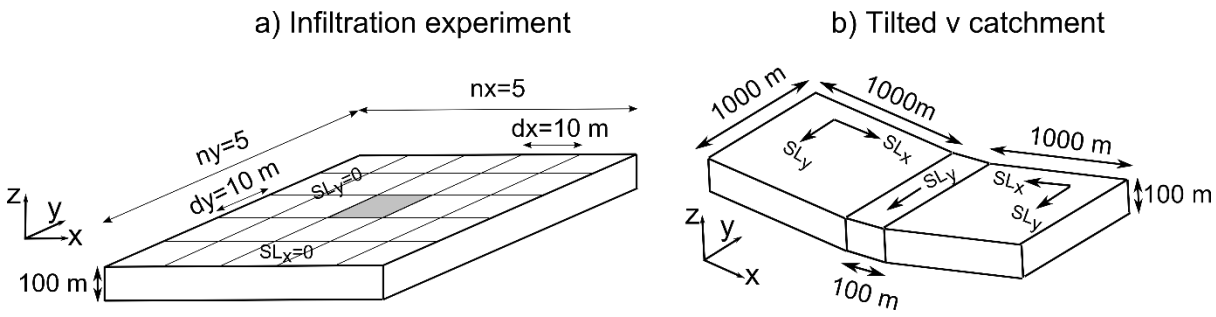

Figure 2. Experimental setup for (a) the infiltration experiment and (b) the tilted-v catchment experiment (not to scale). Note that the total subsurface depth is 100 m in both FULL and GFB (10 m soil and 90 m aquifer) configurations. The FD configuration, in contrast, considers a total subsurface depth of 10 m with a gravity drainage lower boundary condition (see Figure 1 for differences in column setup for all cases). Figure 3-6 show results from the central cell of Figure 2a (shown in grey).

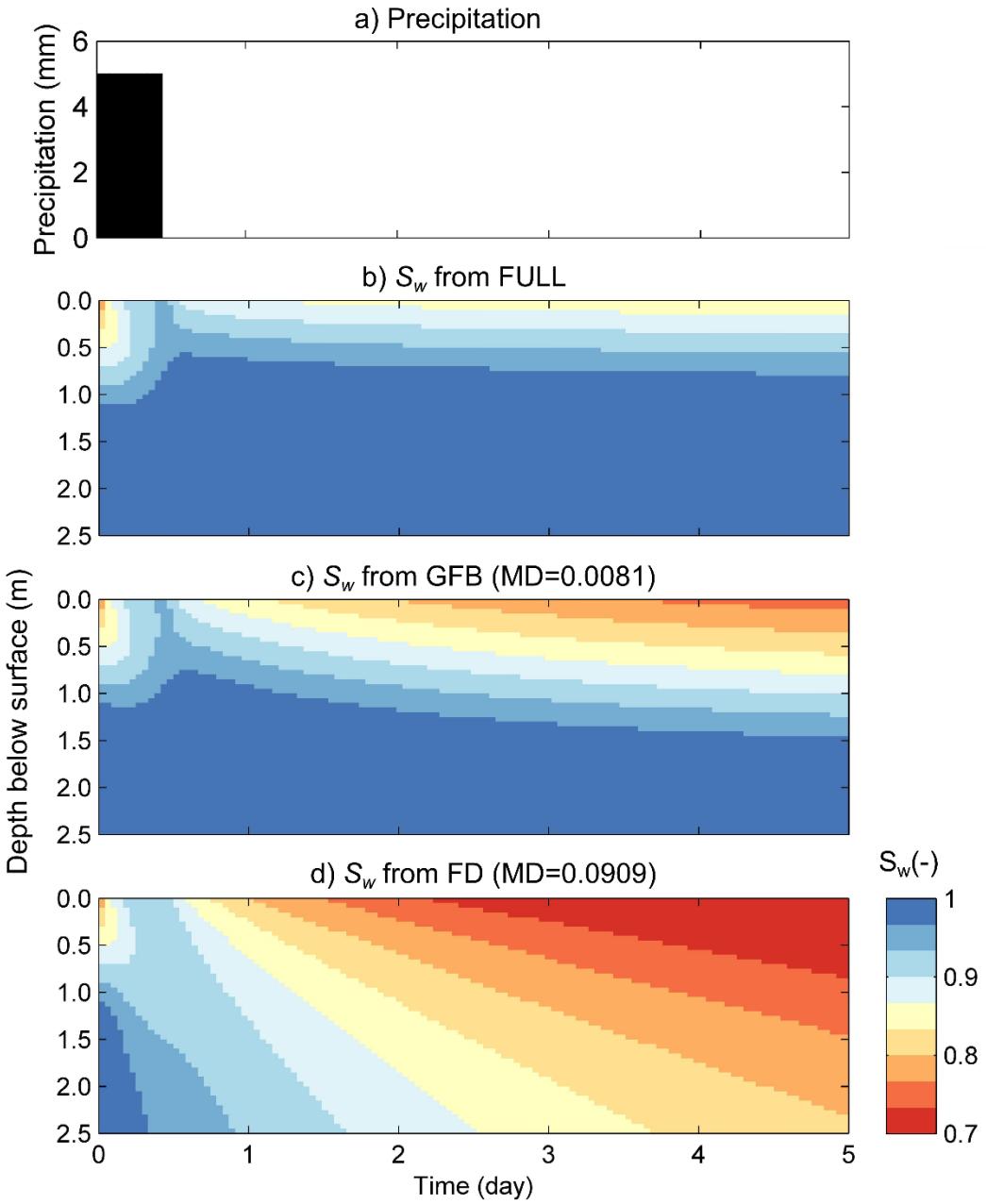

601

602 Figure 3. (a) Spatially uniform hourly precipitation applied in the infiltration experiment;
603 hourly relative soil moisture (S_w) profiles from (b) FULL, (c) GFB, and (d) FD model
604 configurations from the infiltration experiment assuming properties from silty soils. Note the
605 Mean Difference (MD) of GFB and FD profiles compared to FULL in the respective figure
606 titles.

607

608

609

610

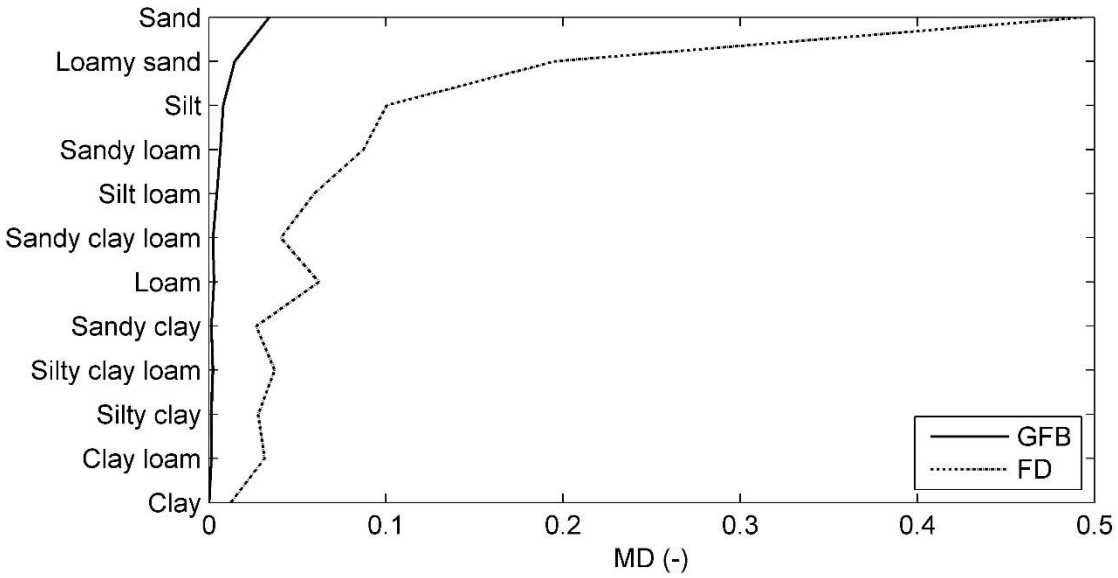

611

612

613 Figure 4. Mean Difference (MD) of GFB and FD simulated S_w profiles compared to FULL

614 for different soil types from the infiltration experiment.

615

616

617

618

619

620

621

622

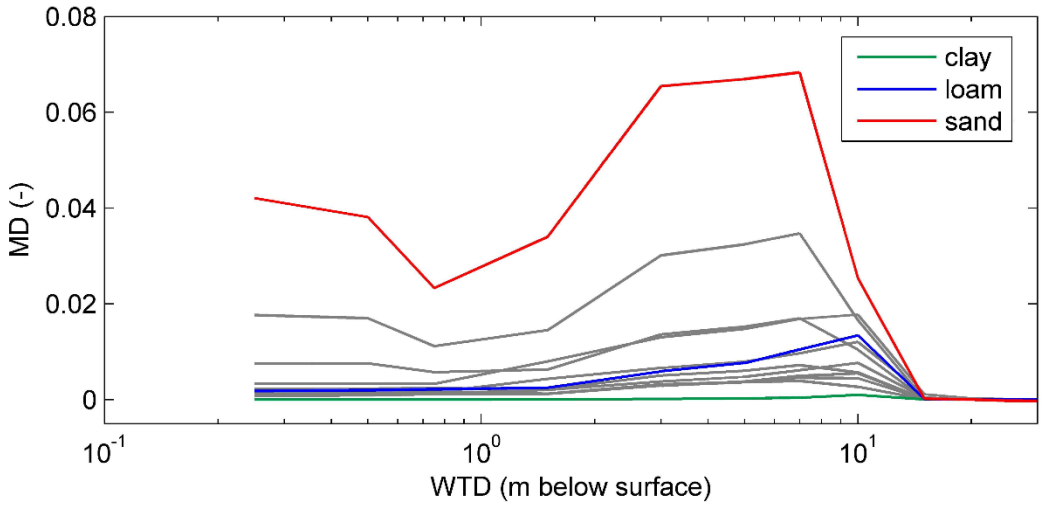

623

624

625

626 Figure 5. Mean Difference (MD) between FULL and GFB simulated S_w profiles considering
627 various Water Table Depth (WTD) initializations and soil types for the infiltration
628 experiment. While sand, loam, and clay are highlighted, results for the other soils are shown
629 in grey.

630

631

632

633

634

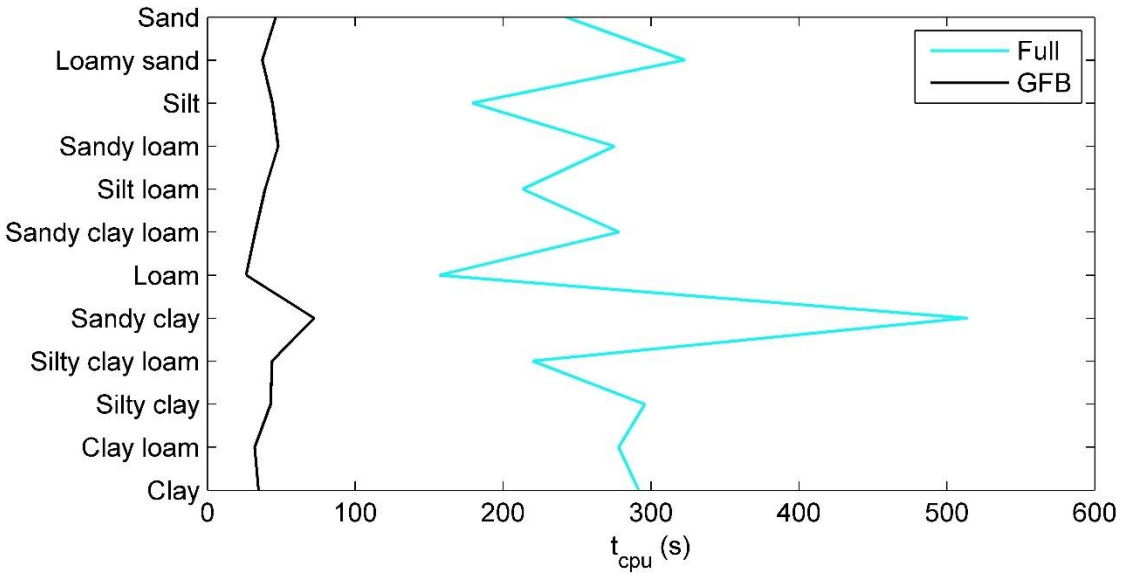

635

636

637

638

639 Figure 6. Required computing time (t_{cpu}) by the FULL and GFB configurations to simulate

640 the infiltration experiment for different soil textural classes.

641

642

643

644

645

646

647

648

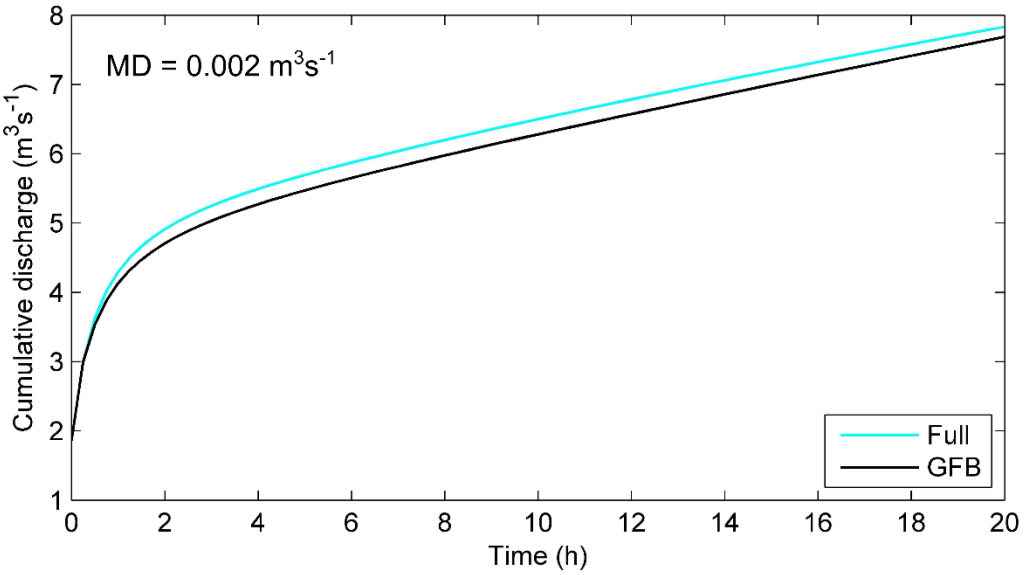

649

650 Figure 7. Cumulative discharge from the FULL and GFB configurations at the outlet of the
651 tilted-v catchment. In this simulation, soil hydraulic properties of loam, SL_x = 0.005, and SL_y
652 = 0.002 are considered. Note the Mean Difference (MD) between the discharge simulated by
653 the two configurations. No rainfall is applied in the tilted-v catchment experiment.

654

655

656

657

658

659

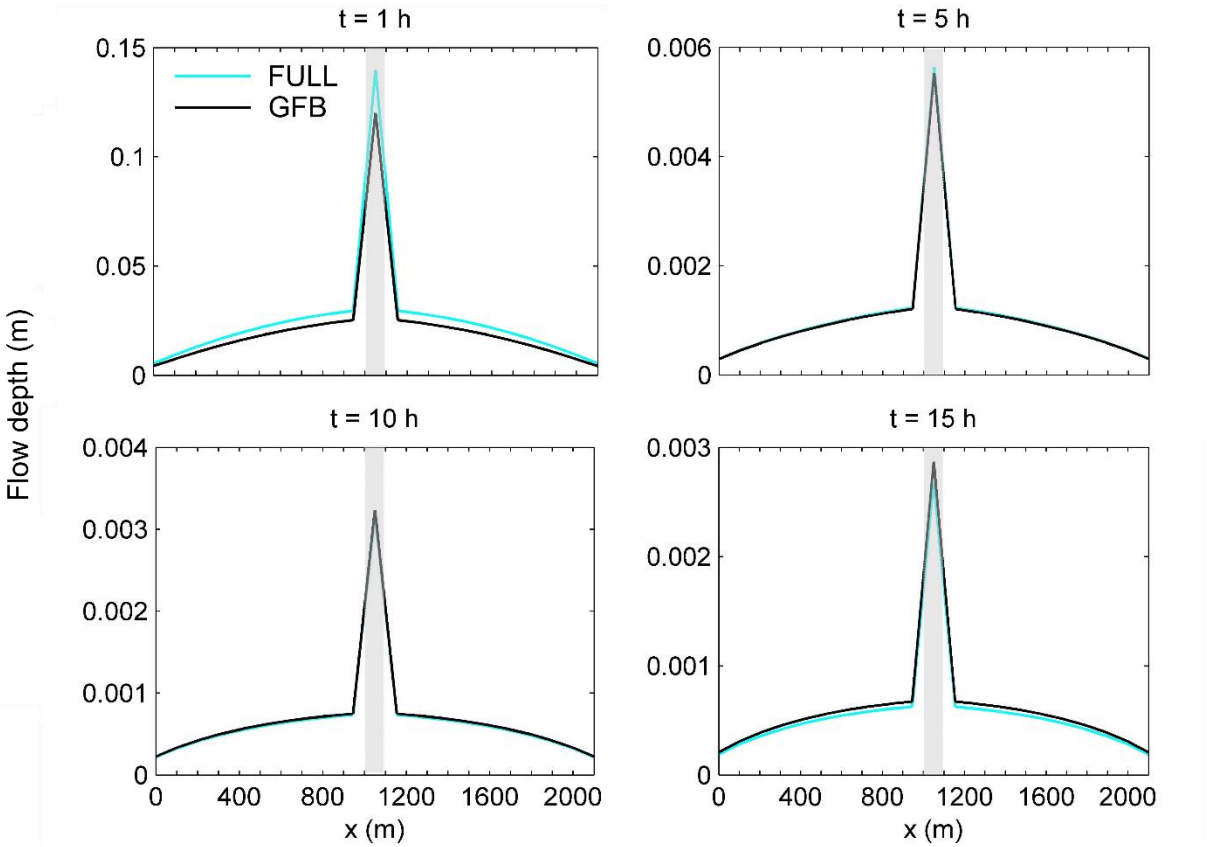

Figure 8. Flow depth along the *x*-axis at *y* = 500 m of the tilted-v catchment (see Figure 2b) for different simulation time instances. The shaded areas in this figure show the locations of the central channel. Note the different scales for the *y*-axes.

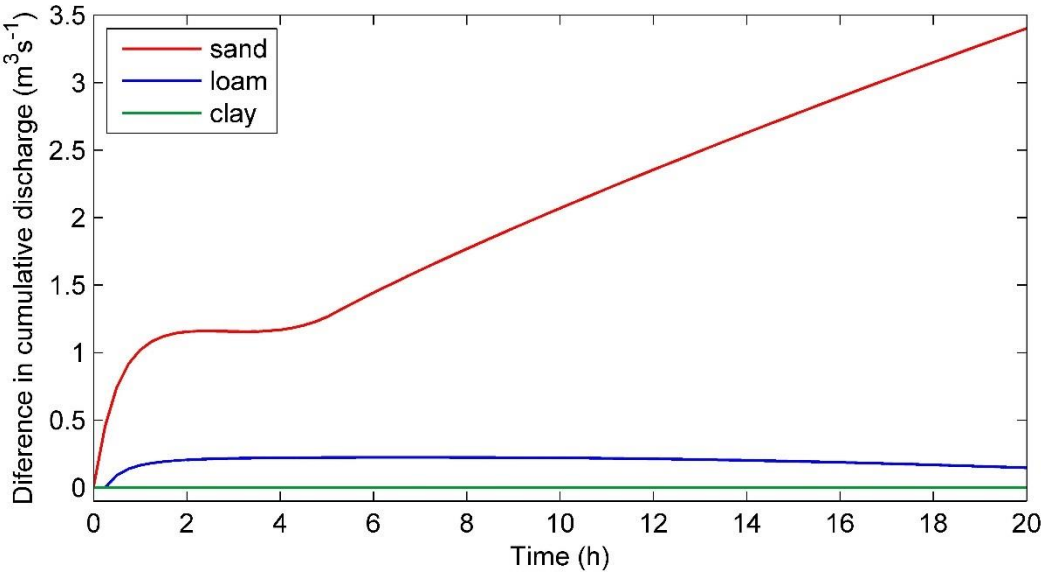

Figure 9. Differences between cumulative discharge from the FULL and GFB configurations at the outlet of the tilted-v catchment for three soil types. In these simulations, $SL_x = 0.005$ and $SL_y = 0.002$ are considered and groundwater table is initially located at the land surface.

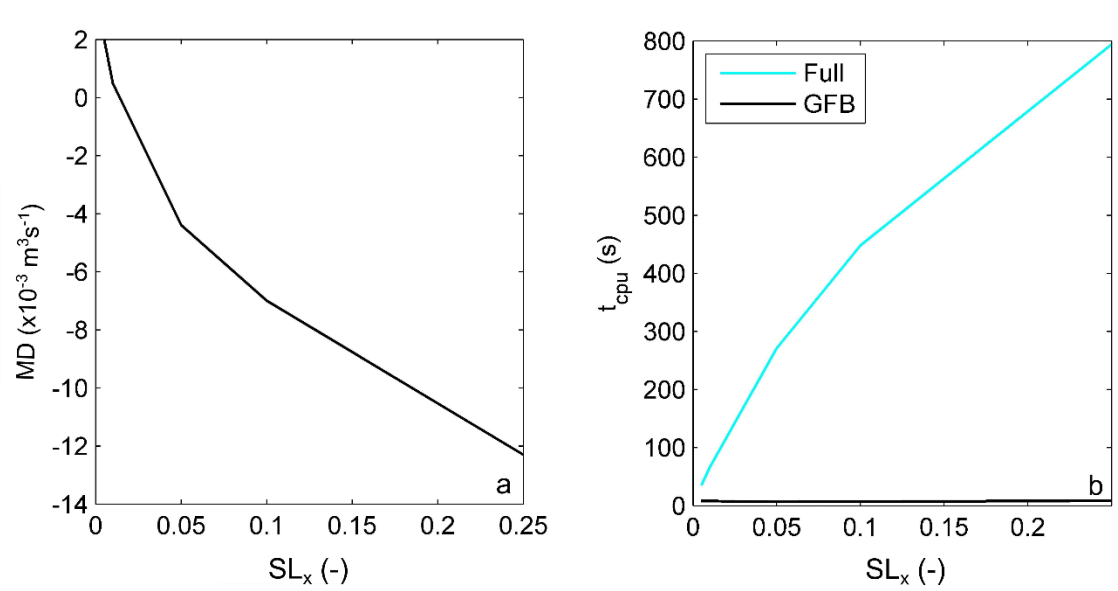

Figure 10. (a) Mean Difference (MD) of GFB simulated discharge at the outlet of tilted-v compared to that of FULL and (b) required computing time (t_{cpu}) by the FULL and GFB configurations to simulate the tilted-v experiment as a function of topographic slope (SL_x). Hydraulic properties of loam soil are considered in this simulation.